

Apolipoprotein A-I mimetic peptide 4F blocks sphingomyelinase-induced LDL aggregation^S

Su Duy Nguyen,* Matti Javanainen,[†] Sami Rissanen,[†] Hongxia Zhao,[§] Jenni Huusko,** Annuikka M. Kivelä,** Seppo Ylä-Herttuala,**^{††} Mohamad Navab,^{§§} Alan M. Fogelman,^{§§} Ilpo Vattulainen,^{†***} Petri T. Kovanen,* and Katariina Öörni^{1,*}

Wihuri Research Institute,* Biomedicum Helsinki, Helsinki, Finland; Department of Physics,[†] Tampere University of Technology, Tampere, Finland; Institute of Biotechnology,[§] University of Helsinki, Helsinki, Finland; A.I. Virtanen Institute for Molecular Sciences, Department of Biotechnology and Molecular Medicine,** University of Eastern Finland, Kuopio, Finland; Science Service Center,^{††} Kuopio University Hospital, Kuopio, Finland; Division of Cardiology, Department of Medicine,^{§§} David Geffen School of Medicine, University of California Los Angeles, Los Angeles, CA; and MEMPHYS-Center for Biomembrane Physics,^{***} University of Southern Denmark, Odense, Denmark

Abstract Lipolytic modification of LDL particles by SMase generates LDL aggregates with a strong affinity for human arterial proteoglycans and may so enhance LDL retention in the arterial wall. Here, we evaluated the effects of apoA-I mimetic peptide 4F on structural and functional properties of the SMase-modified LDL particles. LDL particles with and without 4F were incubated with SMase, after which their aggregation, structure, and proteoglycan binding were analyzed. At a molar ratio of L-4F to apoB-100 of 2.5 to 20:1, 4F dose-dependently inhibited SMase-induced LDL aggregation. At a molar ratio of 20:1, SMase-induced aggregation was fully blocked. Binding of 4F to LDL particles inhibited SMase-induced hydrolysis of LDL by 10% and prevented SMase-induced LDL aggregation. In addition, the binding of the SMase-modified LDL particles to human aortic proteoglycans was dose-dependently inhibited by pretreating LDL with 4F. The 4F stabilized apoB-100 conformation and inhibited SMase-induced conformational changes of apoB-100. Molecular dynamic simulations showed that upon binding to protein-free LDL surface, 4F locally alters membrane order and fluidity and induces structural changes to the lipid layer. Collectively, 4F stabilizes LDL particles by preventing the SMase-induced conformational changes in apoB-100 and so blocks SMase-induced LDL aggregation and the resulting increase in LDL retention.—Nguyen, S. D., M. Javanainen, S. Rissanen, H. Zhao, J. Huusko, A. M. Kivelä, S. Ylä-Herttuala, M. Navab, A. M. Fogelman, I. Vattulainen, P. T. Kovanen, and K. Öörni. **Apolipoprotein A-I mimetic peptide 4F blocks sphingomyelinase-induced LDL aggregation.** *J. Lipid Res.* 2015. 56: 1206–1221.

Supplementary key words low density lipoprotein • apolipoprotein B-100 • proteoglycans • retention • atherosclerosis • conformation • interaction

Subendothelial retention of LDL by the proteoglycans of the extracellular matrix is the key initiating event in the development of atherosclerosis (1, 2). Modification of the retained LDL by lipolytic and proteolytic enzymes present in the arterial intima induces aggregation and/or fusion of the modified LDL particles (3). Aggregation of LDL particles increases their binding strength to the proteoglycans, thus enhancing the extracellular retention of LDL in the arterial intima (3, 4). SMase, an enzyme locally secreted by endothelial cells and macrophages in the arteries (5, 6), has been shown to be one of the enzymes responsible for LDL aggregation during atherogenesis (3). Actually, LDL particles isolated from atherosclerotic arteries resemble LDL aggregates generated by incubation of LDL with SMase in vitro (7). Importantly, genetic deficiency of secretory SMase associates with a reduction of intimal lipoprotein retention and atherosclerotic lesions in mice, thereby providing evidence for a causal role for secretory SMase in the development of atherosclerotic lesions in vivo (8).

Therapeutic strategies to treat atherosclerosis have been developed using apoA-I mimetic peptides (9). These 18 amino acid peptides have no sequence homology to apoA-I, but they possess the same class A amphipathic

The Wihuri Research Institute is maintained by the Jenny and Antti Wihuri Foundation. This study was also supported by the Academy of Finland (K.Ö., S.D.N., M.J., S.R., and I.V.) and the European Research Council (I.V.). M.J. thanks the Finnish Doctoral Programme in Computational Sciences for funding. CSC-IT Center for Science and TCSG-Tampere Center for Scientific Computing are thanked for excellent computational resources. Disclosures: A.M.F. and M.N. are principals in Bruin Pharma, and A.M.F. is an officer in Bruin Pharma.

Manuscript received 25 March 2015.

Published, JLR Papers in Press, April 10, 2015
DOI 10.1194/jlr.M059485

Abbreviations: bcSMase, *Bacillus cereus* SMase; CD, circular dichroism; DLS, dynamic light scattering; hSMase, human recombinant SMase; PLC, phospholipase C; SEC, size-exclusion chromatography; Trp, tryptophan.

¹To whom correspondence should be addressed.

e-mail: kati.oorni@wri.fi

^SThe online version of this article (available at <http://www.jlr.org>) contains supplementary data in the form of seven figures and Materials and Methods.

helical structure as apoA-I (10–13). Among this family of apoA-I mimetics, the most extensively studied peptide 4F is composed of 18 amino acids with the sequence of Ac-D-W-F-K-A-F-Y-D-K-V-A-E-K-F-K-E-A-F-NH₂ (10, 12). The 4F peptide functionally mimics many of the biological properties of apoA-I, and it is both anti-inflammatory and antiatherogenic (10–13). In various mouse models of atherosclerosis, 4F significantly reduced the development of atherosclerotic lesions, being most effective during early atherogenesis (14, 15).

Several potential mechanisms by which 4F might exert its antiatherogenic properties have been proposed. The 4F peptide induces HDL remodeling, which includes formation of pre- β -HDL with elevated paraoxonase activity, and results in promotion of cholesterol efflux and conversion of proinflammatory HDL into anti-inflammatory HDL (14). The antiatherogenic properties of 4F most likely involve binding and sequestering oxidized lipids, which play a critical role in atherosclerosis (16). Indeed, 4F avidly binds to oxidized phospholipids and oxidized unsaturated fatty acids with affinity four to six orders of magnitude higher than apoA-I (17). Given the high affinity of 4F for oxidized phospholipids, which might be present in undetectable amounts in freshly isolated lipoproteins (18, 19), it is plausible to assume that an apoA-I mimetic peptide would also bind to LDL particles. Indeed, 4F was shown to bind to LDL particles, especially when LDL was supplemented with oxidized lipids (20). Moreover, previous studies have demonstrated that amphipathic α -helix-containing apos block phospholipase C (PLC)-induced LDL aggregation (21, 22). Based on the previous information, we hypothesized that 4F would affect the susceptibility of LDL to SMase-induced aggregation. We found that 4F interacts with LDL particles and stabilizes them by preventing SMase-induced conformational changes in apoB-100 and can ultimately block SMase-induced LDL aggregation and the resulting increase in LDL retention.

MATERIALS AND METHODS

Peptides

The amino acid sequence of L-4F is Ac-DWFKAFYDKVAEK-FKEAF-NH₂. The inactive control peptide called scrambled L-4F has the same overall amino acid composition as L-4F but in a sequence that does not promote amphipathic α -helix formation (Ac-DWFAKDYFKKAFVEEFAK-NH₂). 4F peptides were synthesized by the solid phase peptide synthesis method previously described (23).

Isolation of LDL

Human plasma was obtained from healthy volunteers (Finnish Red Cross Blood Service). LDL from human or mouse plasma ($d = 1.019$ – 1.050 g/ml) was isolated by sequential ultracentrifugation (24) or by rapid sequential flotation ultracentrifugation using KBR for density adjustment (25). Lipoprotein stock solutions were dialyzed against LDL buffer (150 mM NaCl, 1 mM EDTA, pH 7.4), filtered, stored at 4°C, and used within 2 weeks, during which no changes in protein conformation and particle size were observed. The amounts of lipoproteins are expressed in terms of their total

protein concentrations, which were determined by BCA protein assay kit (Pierce, Rockford, IL) using BSA as the standard.

Incubation of 4F with LDL

To evaluate the effects of the peptides on SMase-induced LDL aggregation, the experiments were performed under several conditions as described subsequently.

Modification of LDL in the presence of 4F. Human LDL particles (1 mg/ml) were incubated with 200 mU/ml (20.8 nM) of *Bacillus cereus* SMase (bcSMase) (Sigma-Aldrich) in 20 mM Tris (pH 7.0) buffer containing 150 mM NaCl, 2 mM CaCl₂, and MgCl₂ at 37°C in the presence or absence of different concentrations of apoA-I mimetic peptide (molar ratio of peptide to apoB-100 ranging from 1:1 to 20:1) for the indicated times. LDL particles (1 mg/ml) were also modified with 50 μ g/ml of human recombinant SMase (a kind gift from Genzyme) in 20 mM MES buffer (pH 5.5–6.5) containing 150 mM NaCl and 50 μ M ZnCl₂ at 37°C in the presence or absence of different concentrations of apoA-I mimetic peptide for the indicated times, after which the lipolysis was stopped by addition of EDTA (final concentration: 10 mM) and samples were placed on ice. The degree of SMase-induced lipolysis was determined by measuring the amounts of phosphorylcholine in the samples using Amplex Red phosphorylcholine kit (Molecular Probes).

Removal of unbound 4F before LDL modification. LDL particles (2 mg/ml) were incubated with L-4F at 10:1 molar ratio of L-4F to apoB-100 in LDL buffer at 37°C for 30 min, followed by extensive dialysis against LDL buffer at 4°C using dialysis membrane with molecular weight cutoff of 12,000–14,000 Da. After removal of the unbound peptides, the L-4F-treated LDL (referred to as 4F-pretreated LDL hereinafter) and control LDL particles (1 mg/ml) that had not been incubated with the 4F peptide were modified with bcSMase as described previously.

Incubation of 4F with SMase-pretreated LDL. LDL particles (1.25 mg/ml) were incubated with 200 mU/ml of bcSMase (Sigma-Aldrich) in 20 mM Tris (pH 7.0) containing 150 mM NaCl, 2 mM CaCl₂, and MgCl₂ at 37°C. After an incubation for 15 min, lipolysis was stopped by the addition of EDTA (final concentration: 10 mM). Native or bcSMase-treated LDL particles (1 mg/ml) were incubated in 20 mM Tris (pH 7.0) containing 150 mM NaCl at 37°C in the presence or absence of L-4F at 10:1 molar ratio of L-4F to apoB-100 for the indicated times.

Analysis of LDL aggregation and enzyme kinetics of 4F-bound LDL particles

Aggregation of the LDL samples modified as described previously was followed by measuring the absorbance of the LDL samples at 405 nm. The sizes of the aggregated particles were determined by dynamic light scattering (DLS) (ZetasizerNano; Malvern) as described previously (26).

The control LDL and 4F-pretreated LDL particles at 10:1 molar ratio of L-4F to apoB-100 (0.1–1.5 mg/ml) were incubated with bcSMase in 20 mM Tris (pH 7.0) containing 150 mM NaCl, 2 mM CaCl₂, and MgCl₂ at 37°C for 30 min, and the degree of SMase-induced lipolysis was determined by Amplex Red phosphorylcholine kit. K_m , V_{max} , and K_{cat} were determined from the Lineweaver-Burk plot. K_{cat} is the turnover number; the number of substrate molecules each enzyme site converts to product per unit time.

Analysis of modified LDL by size-exclusion chromatography

The fast-protein liquid chromatography profiles of control LDL and LDL modified under different conditions were analyzed using a high-resolution size-exclusion chromatography (SEC) Superose HR6 column connected to the ÄKTA chromatography system (GE Healthcare). The samples were centrifuged

at 10,000 g for 10 min at 4°C, and a 50 µl aliquot of the supernatant was injected into the column and eluted with PBS buffer at a flow rate of 0.5 ml/min. The degree of aggregation is expressed as a percentage of the 280 nm absorbance of peak I of modified LDL to the 280 nm absorbance of peak I of control LDL. Peak areas were calculated by integration of the 280 nm absorbance using the Unicorn 5.2 software.

Circular dichroism spectroscopy

The control and 4F-pretreated LDL particles (1 mg/ml) were modified with bcSMase in 20 mM Tris (pH 7.0) buffer containing 150 mM NaCl, 2 mM MgCl₂, and 2 mM CaCl₂. Samples of control LDL and 4F-pretreated LDL (50 µg/ml) were analyzed by circular dichroism (CD) at different time points as described previously (26, 27).

Tryptophan fluorescence spectroscopy

Fluorescence emission spectra were measured for control LDL or 4F-pretreated LDL particles (0.1 mg/ml) in 20 mM Tris (pH 7.0) buffer containing 150 mM NaCl, 2 mM MgCl₂, and 2 mM CaCl₂ using a PerkinElmer LS 55 Fluorescence Spectrometer. The fluorescence cell holder was thermostatically maintained at 37 ± 0.1°C. The spectra were recorded from 305 to 450 nm with excitation at 295 nm and 5 nm bandwidth for excitation and emission. For each sample, 10 spectra were averaged, and blank measurements were subtracted.

Preparation and characterization of human aortic proteoglycans

Proteoglycans from the intima media of human aortas obtained at autopsy within 24 h of accidental death were prepared essentially by the method of Hurt-Camejo et al. (28) and characterized as previously (29).

Binding of human LDL to proteoglycans

To examine the effect of 4F on the ability of SMase-modified LDL to bind to human aortic proteoglycans, control LDL and 4F-pretreated LDL particles (molar ratio of peptide to apoB-100 ranging from 2.5:1 to 20:1) were modified with bcSMase for 15 min in 20 mM Tris (pH 7.0) buffer containing 150 mM NaCl, 2 mM MgCl₂, and 2 mM CaCl₂. Aliquots of the control and 4F-pretreated LDL particles were used for proteoglycan binding study.

The wells in polystyrene 96-well plates were coated with 100 µl of human aortic proteoglycans (50 µg/ml) or fatty acid-free BSA (5 mg/ml) at 4°C overnight and blocked with 5% fatty acid-free BSA, 1% fat-free milk powder, and 0.05% Tween 20 in PBS for 1 h at 37°C as described previously (4). The LDL aliquots were added to the proteoglycan- or BSA-coated wells in 20 mM Tris (pH 7.0) buffer containing 150 mM NaCl, 2 mM MgCl₂, and 2 mM CaCl₂ and 1% fatty acid-free BSA, and the plate was incubated

for 1 h at 37°C. Unbound LDL particles were removed, and the wells were washed with 20 mM Tris (pH 7.0) buffer containing 30 mM NaCl, 2 mM MgCl₂, and 2 mM CaCl₂, and the bound lipoproteins were detected by a commercial cholesterol kit (Amplex Red; Molecular Probes). Specific binding to proteoglycans was calculated by subtracting the amounts of the lipoproteins bound to the BSA-coated wells from the amounts of lipoproteins bound to the proteoglycan-coated wells.

Animal study

Animal experiments and the protocols were approved by the National Animal Experiment Board. The effect of the peptide on LDL aggregation *in vivo* was studied in 5-month-old male LDLR^{-/-}ApoB^{100/100} mice fed with a high-fat, Western-type diet (TD 88173; Harlan Teklad) for 6 weeks. The peptides were dissolved in DMSO, further diluted into NaCl, and 100 µg/mouse of either L-4F (n = 7) or only DMSO (control, n = 6) was injected via tail vein in 150 µl volume. For the injection, the mice were gently sedated with xylazine (0.1 mg/10 g) and ketamin (0.8 mg/10 g). One hour after the injection, the animals were euthanized, and EDTA-Plasma was collected for LDL isolation. LDL particles (0.15 mg/ml) were incubated with 200 mU/ml bcSMase (Sigma-Aldrich) in 20 mM Tris (pH 7.0) buffer containing 150 mM NaCl, 2 mM CaCl₂, and MgCl₂ at 37°C for indicated times. The sizes of the LDL particles were determined by DLS (Zetasizer-Nano; Malvern).

Atomistic molecular dynamics simulations

Models. To study the interactions of 4F with LDL lipids, planar trilayer systems were computationally used as a model for protein-free LDL. The lipids used in the model (see below) were POPC, palmitoyl SM, cholesterol, cholesteryl oleate, and ceramide, whose structures are well known. The model for the structure of the 4F peptide was obtained as a homology model (L3F, L14F) from the 2F peptide (30) (PDB entry 2F95) by using the Bodil software (31). The trilayer-4F system was surrounded by water with salt (NaCl; see below).

The force fields for POPC, SM, and cholesterol were taken from the Slipids parameter set (32–34), whereas cholesteryl oleate and ceramide were parameterized to be compatible with it (see supplementary Materials and Methods). The Amber03 force field was used for the peptides, and the TIP3P model was used for water (35). All simulations reported in this paper were performed with the GROMACS 4.6.x simulation package (36).

Molecular dynamics simulation setup. The peptide structure was equilibrated by simulating it in water and simultaneously gradually removing restraints from its structure (*Peptide_water* simulations in **Table 1**). The heavy atoms were first restrained for 100 ps followed by a 20 ns simulation with the backbone atoms restrained. Finally, the unrestrained peptide structure was allowed to relax in water for either 20 ns or 1 µs (see below).

TABLE 1. The names, descriptions, and durations of the atomistic simulations in this study

Simulation Set	Configuration and Simulations	Duration
<i>Trilayer_equil</i>	Both trilayer models (with ceramide and with SM) equilibrated in experimental surface tension without the peptide present.	Both trilayers: 650 ns
<i>Peptide_water</i>	The 4F peptide simulated in water, while the restraints were gradually discarded.	100 ps + 20 ns + 1 µs/20 ns
<i>Helix_trilayer</i>	Two helical peptides interacting with the trilayers. Six simulations (one extended) with varying initial configurations for both SM and ceramide.	Both trilayers: 5 × (150/200 ns) + 600 ns
<i>Unfolded_trilayer</i>	One peptide interacting with the trilayers. The partially unfolded peptide structure was taken from the end of the <i>Peptide_water</i> simulation.	Both trilayers: 400 ns
<i>Free_energy</i>	A total of 21 umbrella windows for both trilayers. One peptide with the trilayer. Initial frames were extracted from the <i>Unfolded_trilayer</i> simulation.	Most windows 50 ns, some extended to 200 ns
<i>Annealing</i>	The end structures of the extended <i>Helix_trilayer</i> simulations for the trilayer with SM heated up and subsequently cooled down.	3 target temperatures, 100 ns each

The trilayer systems were constructed by placing a preequilibrated cholesteryl oleate slab of 200 molecules between two lipid monolayers. Each of the monolayers consisted of 100 lipids and their composition followed that of the LDL surface monolayer (37) with 46 mol% POPC, 17 mol% SM, and 37 mol% cholesterol. In the model for SMase-treated LDL, all SM was replaced by ceramide. The systems were hydrated with 50 water molecules per surface monolayer lipid. NaCl (150 mM) was added to the water phase. The system was allowed to relax to the experimental surface pressure (*Trilayer_equl* simulations in Table 1; see also supplementary Materials and Methods for details) before the production simulations with the peptide.

After these relaxation simulations, the peptides were included in the system. We considered two situations: a lipid trilayer corresponding to an unmodified LDL composition (with SM) and a system corresponding to the SMase-treated LDL composition (ceramide replacing SM). Multiple simulations with varying initial conditions were performed to study the interaction of the 4F peptide with these two trilayers: either the interaction of a single partially unfolded peptide with the trilayer was considered, or two almost helical peptides were included into the system simultaneously. In addition, umbrella sampling simulations were performed.

In the single peptide case, called *Unfolded_trilayer* in Table 1, the structure of 4F after 1 μ s of the *Peptide_water* simulation was included in the trilayer systems. For more information on the construction of these initial structures, see supplementary Materials and Methods. The constructed systems were simulated for 400 ns. Snapshots of these trajectories were further used in the umbrella sampling simulations (see below).

Additional data were collected by placing two almost perfectly helical 4F peptides (structure after 20 ns of *Peptide_water* simulation) in the trilayer systems. For more details on the construction of these systems, see supplementary Materials and Methods. These systems are referred to as *Helix_trilayer* in Table 1. Six initial configurations with systematically varying position and orientation of the peptide were considered for both trilayer compositions. These simulations were run until the peptides properly bound to the trilayers. In most replicas, 150 ns was adequate, yet in some cases the simulations needed to be extended to 200 ns. Additionally, one system with each composition was extended to 600 ns in order to observe long-time lipid rearrangement on the trilayer surface. The last 400 ns of these extended simulations was considered in the analysis.

The free energy profiles of the peptide interacting with the trilayers were obtained from umbrella sampling simulations, listed as *Free_energy* in Table 1. The initial structures were extracted from the *Unfolded_trilayer* simulations. The distance between the centers of mass of the peptide and the trilayer in the umbrella windows varied between 1 and 5 nm with a spacing of 0.2 nm. This distance was measured in the direction normal to the trilayer surface. A force constant of 500 kJ/mol/nm² was used for the harmonic restraining potential. The umbrella windows were simulated for 50 ns except for the distances between 3 and 4 nm for which the simulations were extended to 200 ns in order to eliminate some interfacial effects. The data collected during the last 25 ns of all simulation windows were used in the analysis.

Additionally, the thermal stability of the 4F conformation on the SM-containing trilayer surface was studied. The final structures of the extended *Helix_trilayer* simulations were used as starting structures for the annealing simulations in which the system was heated up and subsequently cooled down. The temperature of the system was linearly increased to either 330, 350, or 370 K during 50 ns after which it was linearly decreased back to 310 K during another 50 ns. These simulations are referred to as *Anneal_in* in Table 1.

The simulation parameters were compatible with the Slipids force field in all of the conducted simulations (see the supplementary Materials and Methods for details). A summary of the performed simulations, which covered approximately 10 μ s, is given in Table 1.

Analysis of atomistic simulation data. The electrostatic potential profile along the trilayer normal was obtained by integrating the partial charge distribution of the system twice. This was performed with a GROMACS tool *g_potential*.

The deuterium order parameter $-S_{CD}$ characterizing lipid hydrocarbon chains' conformational order is defined as

$$-S_{CD} = -\frac{3}{2}(\cos^2\theta - 1)$$

Here, θ is the angle between a carbon in the lipid tail and a hydrogen atom (deuterium in an experimental setup, hence the name) bound to it. The angular brackets stand for time and ensemble averages. A value of 0.5 for $-S_{CD}$ refers to perfectly straightened hydrocarbon tails, whereas a value of 0 corresponds in practice to random orientation of the tails. Here, the $-S_{CD}$ profile along the lipid tails was computed from the positions of the tail carbon atoms with the GROMACS tool *g_order*.

Spatially resolved deuterium order parameters were calculated with the *g_lomepro* tool (38). This tool assigns all lipids to grid points in the monolayer plane based on their location. The average ordering at each grid point is presented as a column of spheres, each of which represents a carbon in the hydrocarbon chain of the studied lipid type. The color of these spheres shows the average order parameter of the corresponding carbon at that grid point, whereas their vertical location shows the average depth at which the corresponding carbon resides in that grid point. The data in each grid point are time-averaged as well as averaged over the multiple lipids visiting this grid point during the simulation.

The helical contents of the peptide were calculated, and the simulation snapshots were rendered with the VMD software.

The free energy profiles were calculated from the umbrella sampling simulations with the GROMACS tool *g_wham*, and the error estimates were evaluated with the bootstrapping analysis (39).

Whenever comparison is made with the peptide-free system, the data covering the last 50 ns of the relaxation simulation (see Materials and Methods) are used for analysis.

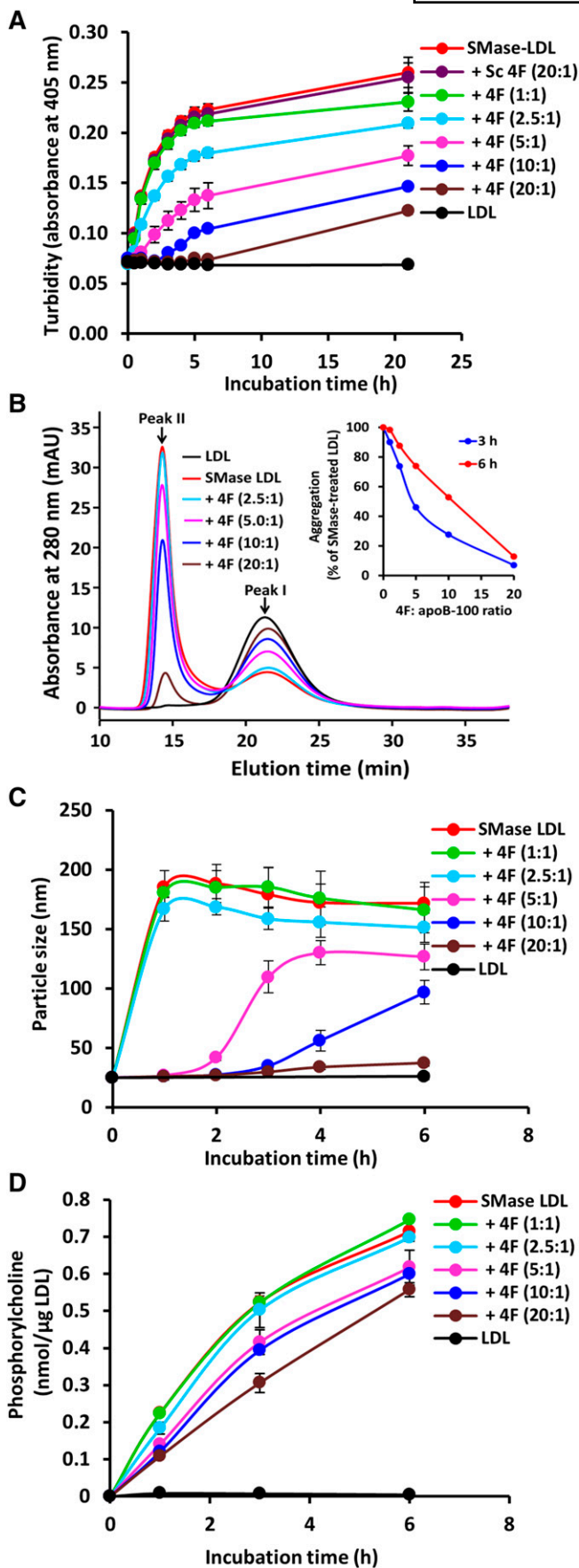
Statistical analysis

Results are reported as mean \pm SD. Statistical significance ($P < 0.05$) was determined by two-tailed Student's *t*-test.

RESULTS

The 4F peptide blocks SMase-induced LDL aggregation

To study the effects of apoA-I mimetic peptides on bcSMase-induced LDL aggregation, LDL particles were first incubated with bcSMase in the absence or presence of 4F. The aggregation and sizes of the lipoprotein particles were measured at various time points. As shown in Fig. 1A, L-4F blocked bcSMase-induced LDL aggregation in a dose-dependent manner as reflected by its ability to prevent an increase in turbidity of bcSMase-treated LDL. At 10:1 or 20:1 molar ratio of 4F to apoB-100, full protection against



SMase-induced LDL aggregation was observed up to 3 h of incubation. With prolonged incubation, the protective role of L-4F gradually diminished, and SMase-induced LDL aggregation increased. In contrast, scrambled 4F did not have any effect on bcSMase-induced LDL aggregation (Fig. 1A). After incubation for 6 h, the ability of 4F to protect against bcSMase-induced aggregation was analyzed by SEC using a Superose 6 HR 10/30 gel filtration column (Fig. 1B). Control LDL, which had been incubated without bcSMase, eluted from the column as a single peak, corresponding to the elution volume of native LDL (peak I). By contrast, the elution profile of SMase-treated LDL showed two peaks. Peak II, which contained aggregated LDL, eluted at the void volume of the column, and peak I eluted at a position corresponding to the elution volume of control LDL. Inclusion of L-4F in the incubation mixture effectively prevented SMase-induced LDL aggregation, as evidenced by a decrease in the amount of LDL eluting in peak II and by an increase in the amount of nonaggregated LDL (peak I). Quantitative analysis of the chromatograms indicated that L-4F exhibited a 72% and 47% protection against SMase-induced LDL aggregation at 10:1 molar ratio of L-4F to apoB-100 after 3 h and 6 h incubation, respectively (Fig. 1B, inset). We further determined the particle sizes of LDL treated with bcSMase in the presence of L-4F using DLS. Consistent with the aggregation data, 4F dose-dependently prevented the formation of larger aggregates (Fig. 1C). Next, we investigated whether inclusion of L-4F in the incubation would affect the susceptibility of LDL particles to bcSMase hydrolysis and found that L-4F decreased the capacity of bcSMase to hydrolyze LDL particles in a dose-dependent manner (Fig. 1D). However, when using pure SM as a substrate, 4F did not inhibit but rather stimulated bcSMase activity, thereby excluding a direct inhibitory effect of 4F on SMase (supplementary Fig. 1). Taken together, the data suggest that 4F interacted with LDL particles and rendered them less susceptible to SMase hydrolysis and thus blocked the SMase-induced LDL aggregation.

The 4F peptide blocks SMase-induced LDL aggregation at acidic pH

We have previously shown that acidic pH enhances SMase-induced LDL aggregation (26). Here, we examined whether L-4F would block SMase-induced LDL aggregation

Fig. 1. The effect of 4F on SMase-induced LDL aggregation during coinubation. LDL particles (1 mg/ml) were modified with bcSMase in the absence or presence of the indicated molar ratios of peptide to apoB-100 at pH 7.0. The aggregation of the LDL particles was monitored by measuring the turbidity (A) and by SEC (B). The inset in B shows quantitative analysis of protection of L-4F against SMase-induced LDL aggregation at 3 and 6 h time points based on the SEC data. The sizes of the LDL particles were measured using DLS (C) at the indicated time points. The SMase-induced formation of phosphorylcholine was determined by an Amplex Red assay (D). The results represent means \pm SD of triplicate wells and are representative of four independent experiments performed with different LDL preparations.

also at acidic pH. For this purpose, LDL was treated with human recombinant SMase (hSMase) at pH values 5.5–6.5 in the presence and absence of different concentrations of L-4F. As expected, inclusion of L-4F in the incubation mixture prevented increase in the turbidity of the mixture (i.e., it blocked hSMase-induced LDL aggregation) (Fig. 2A). SEC data further confirmed that L-4F possesses the ability to prevent hSMase-induced LDL aggregation (Fig. 2B). Particle size measurement revealed that 4F prevented the formation of large aggregates at acidic pH (Fig. 2C). Similar to the data observed at neutral pH, we found that 4F also diminished the capacity of hSMase to hydrolyze LDL particles at acidic pH (Fig. 2D).

The 4F-pretreated LDL particles are resistant to SMase-induced LDL aggregation

Next, we examined whether removal of unbound 4F before incubation of LDL with bcSMase would maintain its

effect on SMase-induced LDL aggregation. To this end, we first incubated LDL particles with L-4F at 10:1 molar ratio of 4F to apoB-100 for 30 min, followed by extensive dialysis to remove unbound L-4F, after which the LDL samples were subjected to modification by bcSMase. Pretreatment of LDL with L-4F protected LDL from bcSMase-induced aggregation in a time-dependent fashion, as demonstrated by turbidity (Fig. 3A), SEC (Fig. 3B), and DLS methods (Fig. 3C). Again, pretreatment of LDL with L-4F decreased the susceptibility of LDL particles to hydrolysis by bcSMase (Fig. 3D). Further detailed analysis of enzyme kinetics indicated that 4F-bound LDL exhibited lower K_m , V_{max} and K_{cat} (Table 2), indicating that binding of 4F to LDL particles effectively hindered the SMase from accessing the SM molecules in LDL particles.

We next studied whether 4F-induced protection from SMase-induced aggregation was solely due to inhibition of SM hydrolysis. For this purpose, LDL particles were first

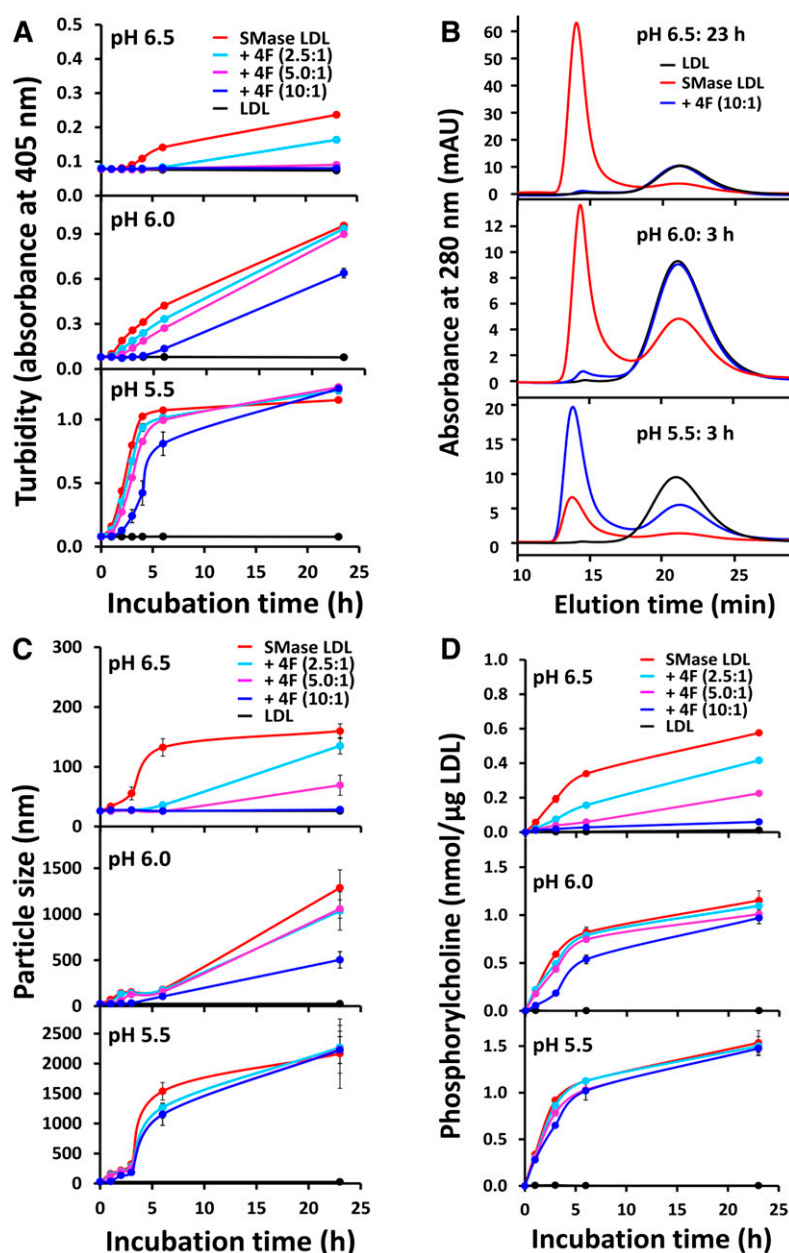


Fig. 2. The effect of 4F on SMase-induced LDL aggregation at acidic pH. LDL particles (1 mg/ml) were modified with hSMase in the absence or presence of the indicated molar ratios of L-4F to apoB-100 at different pH. The aggregation of the LDL particles was monitored by turbidity (A) and by SEC (B). The sizes of the LDL particles were measured using DLS (C) at the indicated time points. The formation of phosphorylcholine was determined by an Amplex Red assay (D). The results represent means \pm SD of triplicate wells and are representative of two independent experiments performed with different LDL preparations.

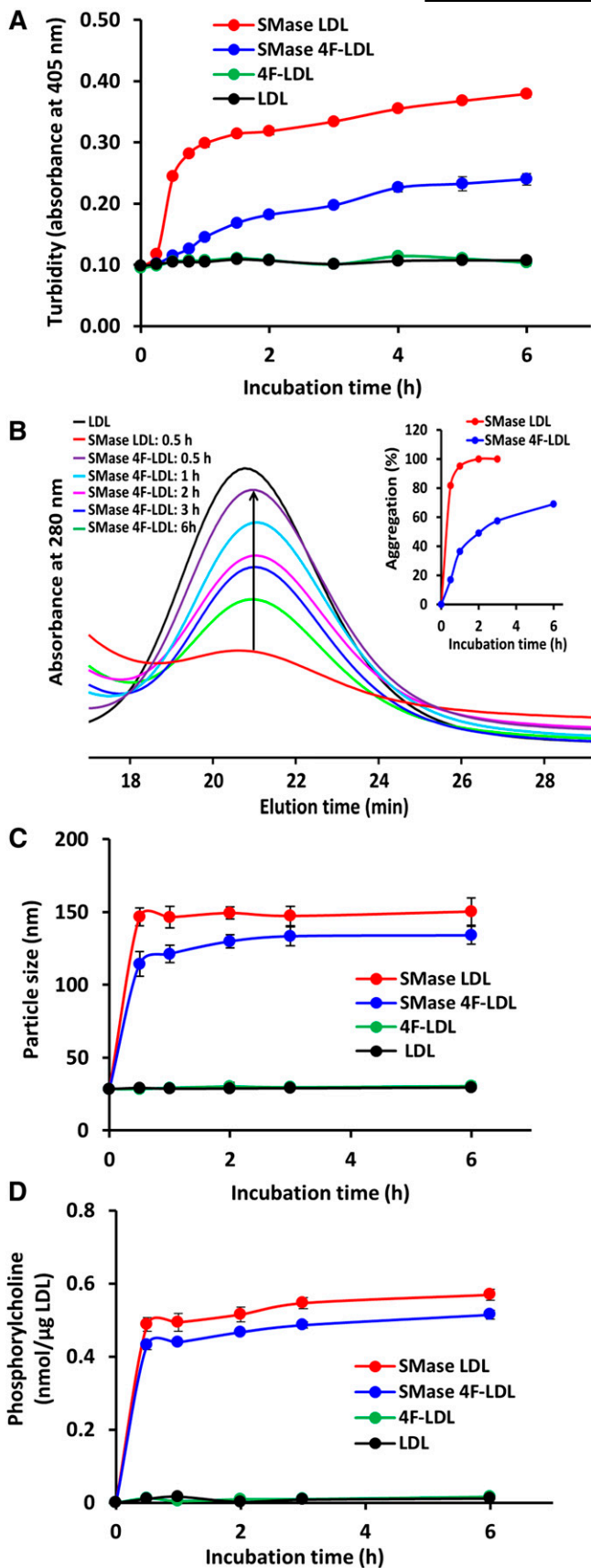


Fig. 3. The 4F-pretreated LDL particles are resistant to SMase-induced LDL aggregation. LDL particles (2 mg/ml) were preincubated with and without L-4F at 10:1 molar ratio of 4F to apoB-100, followed by extensive dialysis. Control and 4F-pretreated LDL

treated with bcSMase for 15 min, followed by the addition of EDTA to fully inhibit the enzyme activity, and finally addition of 4F to the incubation mixture. Under these conditions, SMase treatment induced aggregation of ~40% of LDL particles. Addition of L-4F to SMase-pretreated LDL prevented LDL from further aggregation, as evidenced by turbidity and by SEC data (Fig. 4A, B). Particle size measurement showed that the addition of L-4F prevented LDL particles from forming larger aggregates (Fig. 4C) but failed to diminish the size of the existing aggregates. Because a previous study has revealed that 4F binds to phospholipid vesicles, where it exerts its lipid-solubilizing ability (23), we investigated whether the protective action of 4F against SMase-induced LDL aggregation could be related to its lipid-solubilizing ability. We found that 4F slightly decreased the turbidity of SMase-treated LDL (supplementary Fig. 2A), possibly due to a minor lipid-solubilizing effect (23). However, when added to SMase-treated LDL, which exhibited almost a maximum degree of aggregation, 4F was unable to diminish the aggregate sizes (supplementary Fig. 2B), indicating that the protective action of 4F was independent of its lipid-solubilizing activity.

The 4F peptide rapidly binds to trilayer models of SMase-treated and untreated LDL

As 4F has been shown to vividly bind to lipid bilayers (23) and also to bind to LDL particles (20), we used atomistic molecular dynamics simulations to investigate the interactions of 4F with LDL lipids in detail using a planar trilayer system mimicking the lipid composition in LDL (Fig. 5A). The key objectives of the simulations were to unlock the forces driving 4F to the LDL surface, estimate the effect of SMase-conducted modifications to the peptide-trilayer binding strength, and unravel how 4F changes the surface properties of LDL prior to and after SMase action. Consideration of the action of SMase on LDL would require quantum-mechanical simulations due to the enzymatic reaction involved, and as these are not feasible, we effectively modeled the role of SMase by considering the situation prior to (system with SM) and after its effect (all SM replaced with ceramide).

First, the 4F peptide was simulated in water (*Peptide_water* simulation) in order to find the correct secondary structure of the peptide in the water phase. The average helical content of the 4F peptide versus time, shown in supplementary Fig. 3A, was calculated to be 50.5% during the last 500 ns of this simulation. This is significantly higher than

(1 mg/ml) were modified with bcSMase at pH 7.0, and the aggregation of the LDL particles was monitored by turbidity (A) and by SEC (B). The inset in B shows quantitative analysis of aggregation based on the SEC data. The sizes of the LDL particles were measured using DLS (C) at the indicated time points. The formation of phosphorylcholine was determined by an Amplex Red assay (D). The results are representative of three independent experiments performed with different LDL preparations.

TABLE 2. The bcSMase kinetic parameters for LDL and 4F-pretreated LDL particles

Substrate	K_m (μM)	V_{max} (nmol/min)	K_{cat} (1/min)
LDL	4.25 ± 0.53	0.11 ± 0.014	54.60 ± 7.12
4F-LDL (10:1)	3.18 ± 0.07^a	0.08 ± 0.001^a	38.08 ± 0.88^a

The control LDL and 4F-pretreated LDL particles at 10:1 molar ratio of L-4F to apoB-100 (0.1–1.5 mg/ml) were incubated with bcSMase. The SMase activity was determined by measuring the amounts of phosphorylcholine. K_m , V_{max} and K_{cat} were determined by Lineweaver-Burk plot.

^a $P < 0.05$ versus LDL.

the experimentally measured value of 12% (40), in line with the tendency of atomistic force fields to favor helical conformations (41, 42).

The equilibrated peptide was then placed in the water phase next to the trilayer. Both trilayer compositions were considered for this *Unfolded_trilayer* simulation. During the simulations, the peptide rapidly bound to trilayer surfaces of both compositions and began to fold back into a more helical structure. At the end of 400 ns simulations, the measured average helical contents, shown in supplementary Fig. 3B, were close to 80% with both trilayer compositions, suggesting a substantial environment-driven conformational change of the peptide. This result suggests that the helical conformation of the peptide is the equilibrium structure on the trilayer surface. This justifies the use of the extended *Helix_trilayer* simulations (in which the helical peptide was observed to bind to the trilayer surface without having time to unfold) in studying the long-time effects of the peptide on the trilayer surface properties (see below).

We increased the number of simulations focusing on the binding process to increase the statistical significance of the findings. However, as the folding of the peptide was quite slow on the trilayer surfaces, we considered (instead of the unfolded case) the helical structure of the peptide as the initial structure that was placed in the vicinity of the trilayer (see Materials Methods). Additionally, to increase sampling in these *Helix_trilayer* simulations, two peptides were placed next to the trilayer instead of just one. Out of a total of 12 simulated replicas (see Materials and Methods), the binding of 4F to the trilayer was observed in almost all of them regardless of whether the trilayer contained ceramide or SM. Additionally, we did not find differences in the binding process or final structures between the peptides with different initial orientations or positions. In two replicas, one of the peptides diffused through the box boundary (allowed by periodic boundary conditions) to bind to the other peptide. Due to their amphipathic nature, they formed a stable dimer that resided in the water phase for the rest of the simulation. In all other replicas, however, the binding of 4F to the trilayer was avid, and the two peptides bound either to different monolayers (i.e., different sides of the trilayer) or to the same monolayer. In the extended simulations (600 ns) considered in some of the further analysis, the peptides were attached to separate monolayers.

To compare the effect of the trilayer composition on the binding process more quantitatively, we performed umbrella sampling simulations to calculate the free energy

profile for the binding process. The free energy profiles, shown in Fig. 5B, display large free energy minima at the trilayer surface regardless of the trilayer composition. These minima lie at ~ 90 kJ/mol that corresponds to almost 40 times the thermal energy at 310 K indicating that the association of 4F to the LDL surface is highly irreversible. The binding to the SM-containing trilayer is slightly more favorable than the binding to the ceramide-containing trilayer, the difference being ~ 7 kJ/mol. The profiles also bring out that the partitioning of the peptide to the trilayer core is very unfavorable as the free energy grows rapidly as the peptide gets closer than 2 nm from the trilayer's center of mass. The location of the free energy minimum at 2.5 nm also corresponds to the average peptide-trilayer distance in the equilibrium simulations, as expected. This penetration depth can be compared with the values obtained by Gorbenko et al. (43) in their fluorescence resonance energy transfer experiments. They measured that a tryptophan (Trp) residue of the Ac-18A-NH₂ peptide, which closely resembles the 4F peptide used in this study, lies at ~ 1.5 – 1.7 nm from the core of a cholesterol-free phosphatidylcholine (PC) bilayer. We measured the distance of the Trp residue of 4F to be 1.3–1.6 nm away from the terminal carbon atoms of the POPC and SM/ceramide tails. This is in good agreement with the experimental value when the much looser packing of our trilayer system compared with a PC bilayer is taken into account.

As the conformation of the peptide was found to strongly depend on the environment (water vs. trilayer surface) and was also assumed to affect the free energy profiles, we allowed the conformation to relax for 25 ns (175 ns for certain windows, see Materials and Methods) prior to data collection. The helical content of the peptide in the umbrella windows, shown with dashed lines in Fig. 5B, shows that the peptide conformation changes quite smoothly upon binding to the trilayer. This increase of helical content close to the trilayer surface suggests that our umbrella sampling windows, even with limited sampling time, capture the binding process properly.

The driving force for the strong adsorption of the peptide appears to be of electrostatic origin complemented by the hydrophobic effect. The importance of electrostatics is highlighted in Fig. 5C, which shows the electrostatic potential profile across the lipid trilayer system. One finds that the electrostatic component of the binding of 4F with the lipid trilayer is the strongest in the unmodified system (with SM) with a dilute 4F concentration, in agreement with the free energy calculations. The binding strength in terms of electrostatics becomes weaker if SM is replaced

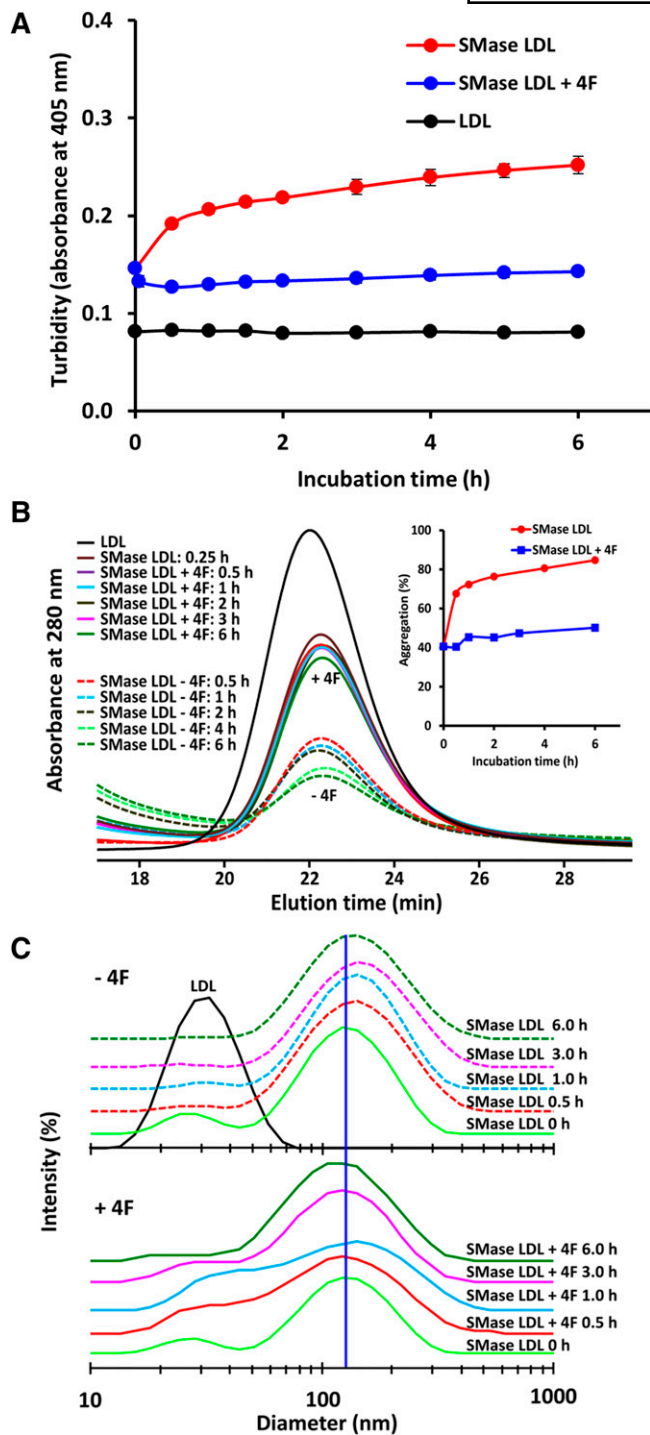


Fig. 4. The effect of 4F on SMase-premodified LDL. LDL particles (1.25 mg/ml) were modified with SMase at pH 7.0 for 15 min after which lipolysis was stopped and the premodified LDL particles (1 mg/ml) were incubated with and without L-4F at 10:1 molar ratio of 4F to apoB-100. The aggregation of the LDL particles was monitored by turbidity (A) and by SEC (B). The inset in B shows quantitative analysis of aggregation based on the SEC data. The sizes of the LDL particles were measured using DLS (C) at the indicated time points. The results are representative of two independent experiments performed with different LDL preparations.

with ceramide, modeling the effect of SMase, or if the concentration of 4F at the membrane surface increases. Yet, in all cases, the driving force for binding due to electrostatic

interactions is substantial, in agreement with experimental data.

The 4F peptide induces structural changes into the lipid trilayer. As shown in Fig. 5D, the deuterium order parameter ($-S_{CD}$) characterizing conformational order in the hydrocarbon chain region increases when 4F binds to the lipid surface. This indicates that 4F makes the membrane more compact by decreasing the amount of free volume in the lipid phase, thus decreasing the average area per lipid, and this takes place in both unmodified (with SM) and modified (with ceramide) lipid systems. We further studied the ordering effect of the peptide by calculating the $-S_{CD}$ of the palmitate chain of POPC on a two-dimensional grid. These spatially resolved order parameters are shown in Fig. 5E for one monolayer in the system containing ceramide, yet the conclusions are also valid for the SM system. The results highlight that upon binding to the lipid layer, 4F increases conformational disorder in lipids that are right under it, but it increases order in lipids outside the binding region, and overall the total conformational order is promoted due to enhanced packing. We conclude that whereas the peptide locally perturbs and disorders the membrane, this causes the lipid packing to increase in regions not covered by the peptide, and these uncovered regions might play a role in LDL aggregation.

The specificity of 4F binding to the lipids was evaluated, yet no tendency for any lipid type was observed even during the extended *Helix_trilayer* simulations (data not shown). This may result from the miscibility of the monolayer components; as there are no domains present within the surface layer, the peptide always interacts with many types of lipids upon binding. The strong electrostatic and hydrophobic interactions as well as the hydrogen bonds formed with the monolayer lipids (data not shown) cause the peptide to bury into the head group region and therefore prevent the peptide from exchanging its close neighbors even in the probed timescales of hundreds of nanoseconds.

The stability of the peptide structure on the trilayer surface was evaluated in the *Annealing* simulations. In these simulations, the peptides remained bound to the trilayer, and their structures remained quite stable. The time evolution of the distance between the trilayer and the peptide and the peptide root mean squared deviation is shown in supplementary Fig. 3C, D.

The 4F peptide stabilizes apoB-100 conformation by binding and perturbing LDL lipids

We further examined the interactions of L-4F with native LDL particles using SEC. Incubation of native LDL particles with 4F at 10:1 molar ratio of 4F to apoB-100 or below did not show apparent changes in the SEC profiles of LDL (Fig. 6A). DLS analysis also revealed that no change in particles size was observed when LDL particles were incubated with L-4F at molar ratio of 20:1 or below (Fig. 6B). However, at 40:1 molar ratio of 4F to apoB-100, significant increase in LDL particle size and remarkable changes in SEC profiles were observed. No signal at 280 nm wavelength was detected when the same concentration of peptide alone was applied to the column, excluding the

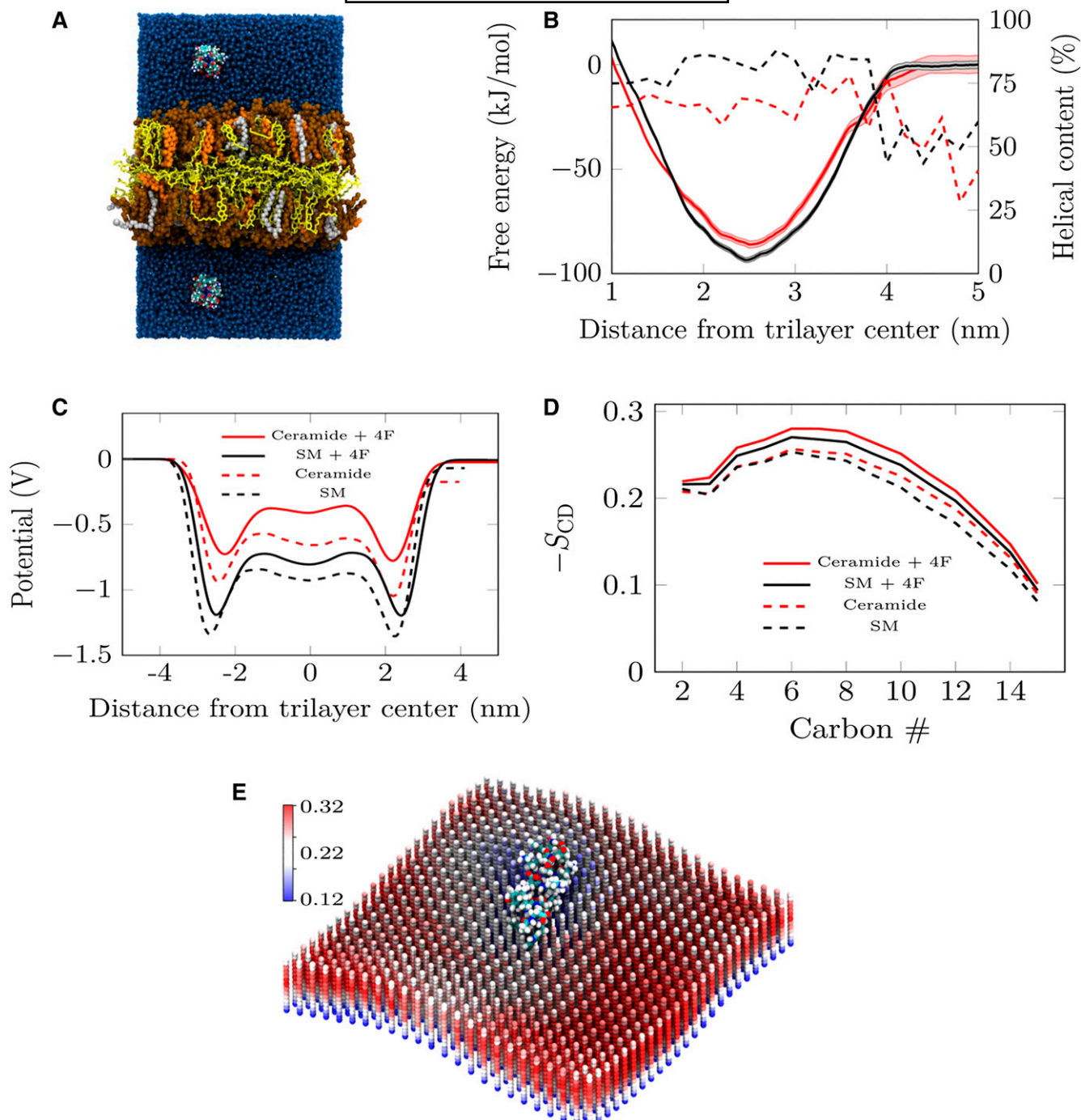


Fig. 5. Atomistic simulations showing that 4F alters the properties of the surface monolayer in protein-free LDL. **A:** Side view of the initial structure of one replica of the *Helix_trilayer* simulations with ceramide. Two 4F peptides are positioned in the water phase in the beginning of the simulation. Cholesteryl oleate is shown in yellow, POPC in brown, cholesterol in orange, and ceramide in gray. Water is shown in blue, and the peptides are depicted with standard atom coloring (carbon, cyan; oxygen, red; hydrogen, white; and nitrogen, blue). **B:** The free energy profiles for the 4F peptide binding to the two trilayer surfaces. Black curves stand for the system with SM (prior to SMase treatment), while red ones show data for the system with ceramide (after SMase treatment). The shaded area shows the statistical error estimated with the bootstrapping analysis. The dashed lines show the average helical contents of the peptide in the umbrella windows. **C:** The electrostatic potential profile across the lipid trilayer system. Red and black curves show data for trilayers containing ceramide and SM, respectively. Dashed lines show results without the bound peptides (one in each leaflet), while solid lines stand for systems with the peptide. **D:** Simulation data for the deuterium order parameter $-S_{CD}$, characterizing conformational order in the hydrocarbon chain region. Results are given for the saturated palmitate chains of POPC with the carbon numbering starting from the carbonyl carbon. Coloring as in C. **E:** The $-S_{CD}$ order parameter values of the palmitate chain of POPC given on a two-dimensional grid. Here, the location of the peptide was kept constant during the analysis to see the local effects induced by 4F binding. Each column represents data averaged in one grid point. The 14 spheres in each column represent the average position of the representative carbon (2nd to 15th carbon in a saturated palmitate chain of POPC), whereas their color represents the $-S_{CD}$ value. The lattice structure shown for lipid positions is due to the lipid order depicted here on a grid and is thus due to visualization only. In practice, the simulated surface monolayers are always in a fluid phase.

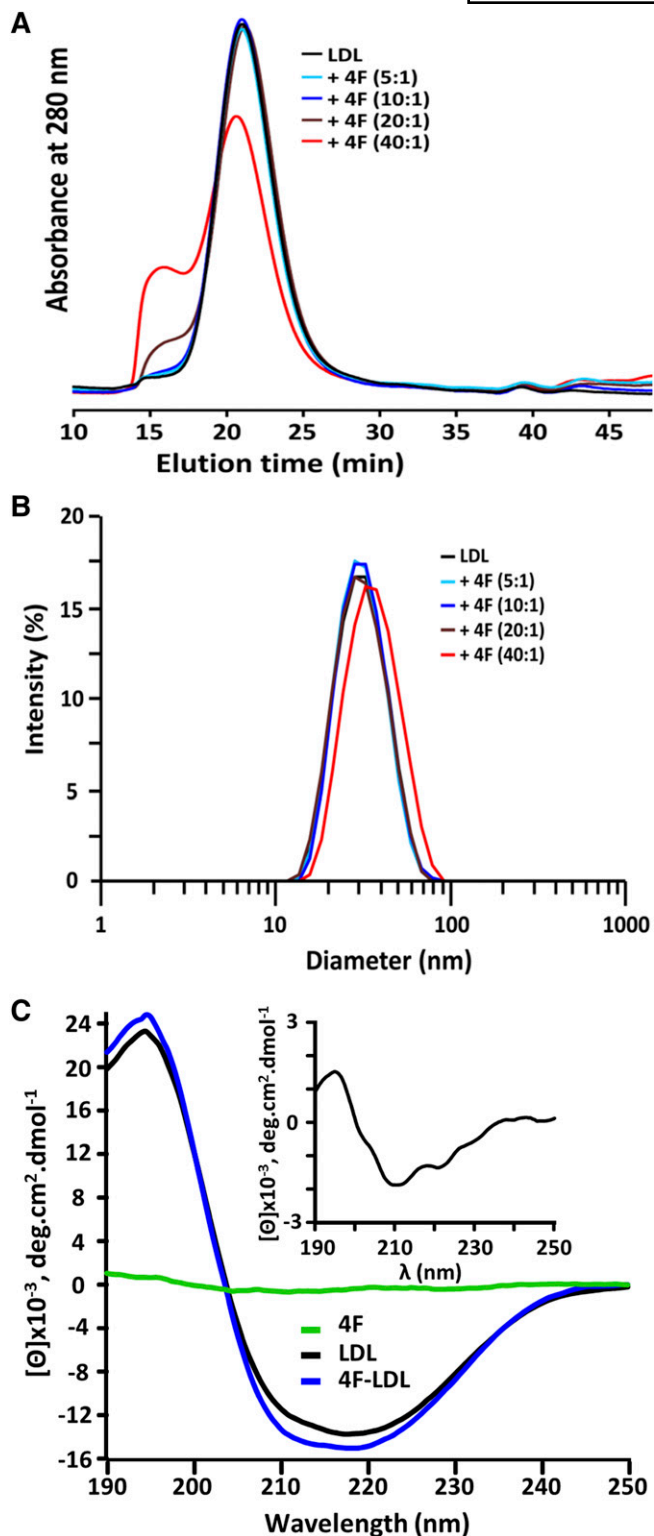


Fig. 6. The effect of 4F on LDL structure. LDL particles (1 mg/ml) were incubated with and without L-4F at the indicated molar ratios of 4F:apoB-100 at pH 7.0 for 30 min. The structure of LDL was analyzed by SEC (A), and the sizes of the LDL particles were measured using DLS (B). LDL (2 mg/ml) was preincubated with and without L-4F at molar ratio of 4F:apoB-100 (10:1), followed by extensive dialysis. The control and 4F-pretreated LDL were diluted to (50 μ g/ml) for far UV-CD measurement (C). The inset in C shows the spectrum difference between 4F-pretreated LDL and LDL: $[\Theta]$ 4F-pretreated LDL - $[\Theta]$ LDL. The green curve indicates the CD signal of the same L-4F concentration that was

possibility that peak II contains peptide oligomers (supplementary Fig. 4A). Cholesterol determination showed that both peaks contained cholesterol-derived LDL, indicating that 4F can destabilize LDL particles at high concentrations (supplementary Fig. 4B).

To further obtain an insight into the mechanism by which 4F blocks LDL aggregation, we studied the effect of 4F on the secondary structure of apoB-100, which has previously been shown to be critical for SMase-induced LDL aggregation (26). We chose the condition at which 4F did not affect LDL particle size but did exhibit its protective action against SMase-induced LDL aggregation. To exclude the contribution of CD of L-4F per se, LDL particles were first pretreated with L-4F at 10:1 molar ratio of 4F to apoB-100 for 30 min, followed by extensive dialysis to remove unbound L-4F. Compared with control LDL particles (Fig. 6C), the spectra of 4F-pretreated LDL have similar shape but show a significant increase in CD intensity, indicating that 4F enhanced the α -helix content of apoB-100 (Fig. 6C). The difference spectrum (inset) showed a positive band at 195 nm and two negative bands at 208 nm and 222 nm, which are characteristics of the α -helix.

Furthermore, intrinsic Trp fluorescence of 4F-pretreated LDL showed a significant increase in fluorescence emission, which probably reflected changes in the Trp microenvironment upon interaction with 4F (supplementary Fig. 5). When the same L-4F concentration was preincubated in buffer alone and directly diluted, even without dialysis, to measure CD and intrinsic Trp fluorescence, no signals were detected (Fig. 6C; supplementary Fig. 5). Collectively, our data indicated that interaction of 4F with LDL particles led to conformational change in apoB-100.

We further investigated whether 4F-induced changes in LDL structure would affect the ability of LDL to bind to LDL receptor of human skin fibroblast. We found that at molar ratio of L-4F to apoB-100 below 20:1, 4F-1,1'-dioctadecyl-3,3,3',3'-tetramethyl-indocarbocyanine perchlorate (DiI)-labeled LDL complex displayed LDL receptor binding similar to control DiI-LDL. However, at a higher concentration of 4F (e.g., 40:1 molar ratio of 4F to apoB-100), 4F-DiI-LDL complex significantly exhibited lower binding to LDL receptor (supplementary Fig. 6).

The 4F peptide prevents SMase-induced conformational changes of apoB-100

Next, the 4F-pretreated LDL and control LDL were subjected to treatment with bcSMase. SMase treatment induced significant conformational changes in apoB-100 as indicated by the decrease in the α -helix content and changes in spectral shape as a function of incubation time with SMase (Fig. 7), corroborating our previous

preincubated in buffer alone and directly diluted without dialysis for CD measurement. The results are representative of three independent experiments performed with different LDL preparations.

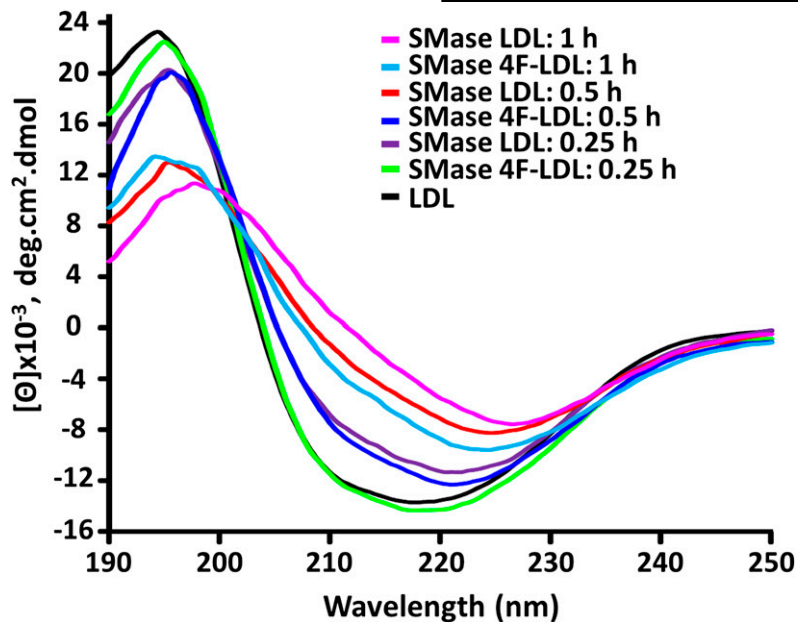


Fig. 7. The 4F peptide prevents SMase-induced conformational changes of apoB-100. LDL particles (2 mg/ml) were incubated with and without L-4F at 10:1 molar ratios of 4F to apoB-100 at pH 7.0 for 30 min, followed by extensive dialysis. Control and 4F-pretreated LDL (1 mg/ml) were modified with bcSMase at pH 7.0 for 15, 30, or 60 min. The samples were diluted to (50 µg/ml) for far UV-CD measurement. The results are representative of two independent experiments performed with different LDL preparations.

finding (26). Importantly, pretreatment of LDL particles with L-4F fully inhibited SMase-induced conformational changes of apoB-100 at 15 min, and the inhibition was gradually diminished after extended incubation times (Fig. 7). Although SMase modification was primarily responsible for conformational changes in apoB-100, we could not completely exclude the possibility that the light-scattering effect of nonuniform particles could contribute to the CD spectral changes of SMase-treated LDL during extended prolongation (over 1 h) when LDL particle size was gradually increased.

The 4F peptide decreases the binding of SMase-treated LDL to human aortic proteoglycans

Because SMase-modified lipoprotein particles bind to human aortic proteoglycans more strongly than native LDL (4), the effects of 4F on the ability of LDL to bind to human aortic proteoglycans were determined. Consistent with our previous study (4), treatment of LDL with bcSMase strongly enhanced the binding of the LDL particles to human aortic proteoglycans (Fig. 8). Interestingly, pretreatment of LDL with 4F significantly decreased binding of SMase-treated LDL to the proteoglycans.

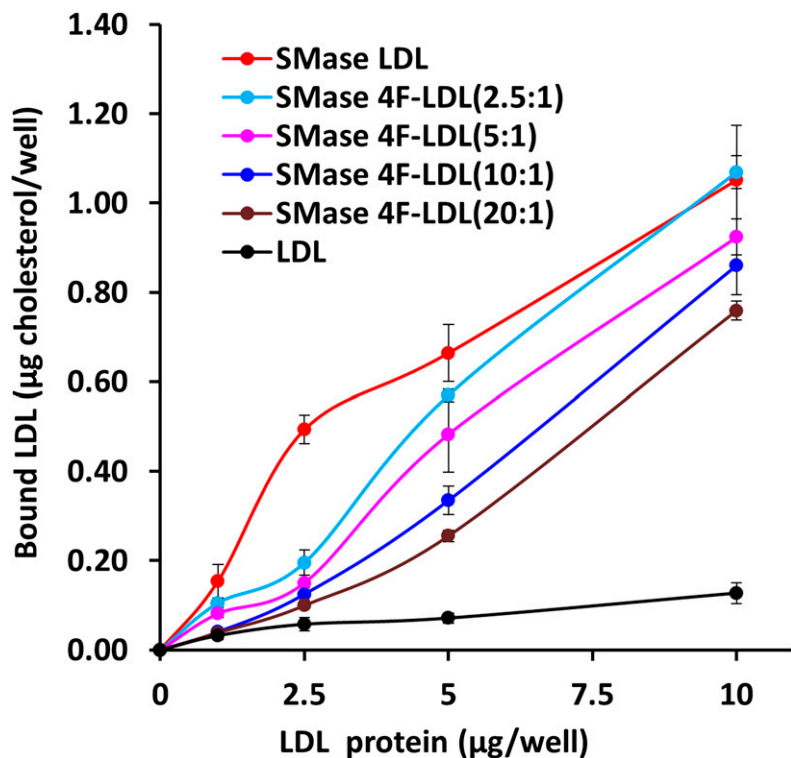


Fig. 8. The 4F peptide decreases the binding of SMase-modified LDL to human aortic proteoglycan. Control and 4F-pretreated LDL particles (1 mg/ml) with molar ratio of L-4F to apoB-100 ranging from 2.5:1 to 20:1 were modified with bcSMase at pH 7.0 for 15 min and aliquots were added to microtiter wells precoated with human aortic proteoglycans. The amounts of proteoglycan-bound LDL were determined by measuring the amounts of cholesterol in the wells. The results represent means \pm SD from triplicate wells and are representative of two independent experiments performed with different LDL preparations.

LDLs isolated from 4F-treated mice are resistant to SMase-induced aggregation

To further study the potential physiological relevance of the observed results *in vitro*, we intravenously injected L-4F (100 $\mu\text{g}/\text{mice}$, the dose corresponding to 20:1 molar ratio of 4F to apoB-100) into LDLR^{-/-}ApoB^{100/100} mice fed with a high-fat, Western-type diet. When LDL isolated from L-4F-treated mice was *ex vivo* modified with SMase, we found that treatment of mice with 4F conferred LDL with ability to resist to SMase-induced aggregation (Fig. 9).

DISCUSSION

In the present study, we have demonstrated that the apoA-I mimetic peptide 4F blocks SMase-induced LDL aggregation and so prevents the SMase-induced increased binding of the modified LDL particles to human aortic

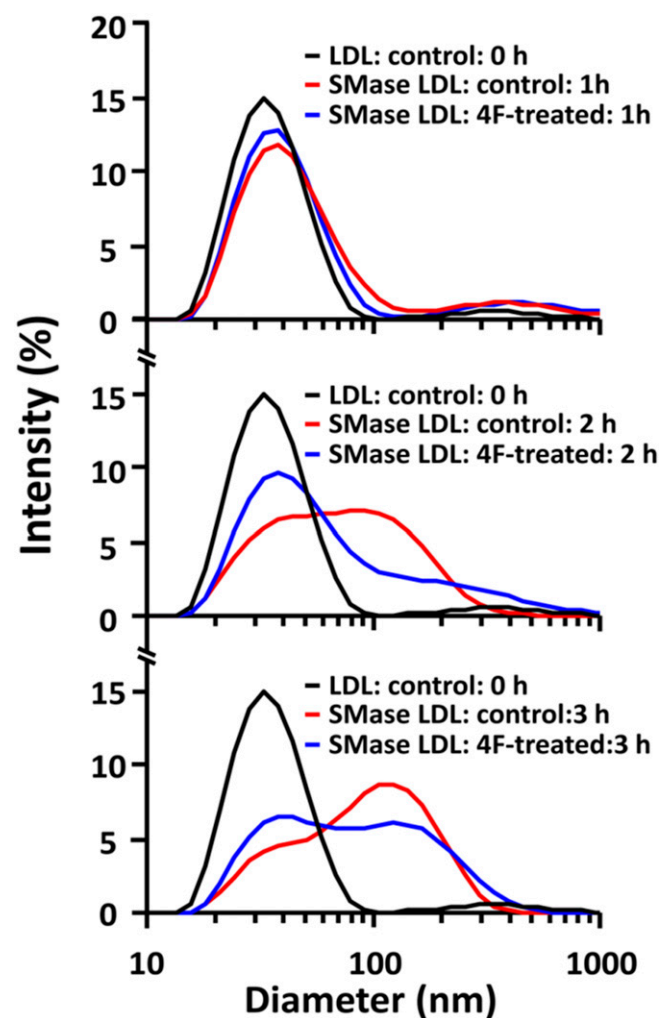


Fig. 9. LDLs isolated from L-4F-treated mice are resistant to SMase-induced aggregation. LDL particles (0.15 mg/ml) from the control or L-4F-treated group were incubated with bcSMase at pH 7.0, and the sizes of the LDL particles were determined by DLS. The results represent average sizes of four different LDL preparations isolated from the control or L-4F-treated group.

proteoglycans. Given the pathological relevance of retention of modified LDL in atherosclerosis (2), our work reveals a novel antiatherogenic functional property of 4F. The data indicate that upon interaction with LDL particles, 4F stabilizes LDL structure and confers LDL particles with the ability to resist SMase-induced LDL aggregation.

The SMase-induced changes in the lipid monolayer of LDL particles lead to remarkable changes in the secondary structure of apoB-100 with a dramatic decrease in its α -helix content (i.e., structural changes pivotal for LDL aggregation) (26). This earlier finding prompted us to define the effects of 4F on the structure of LDL particles. We found that following interactions with 4F, the α -helix content and Trp fluorescence of apoB-100 in LDL particles was slightly enhanced, indicating the local conformational changes in LDL structure. As a result, 4F enhanced the resistance of LDL particles to SMase-induced alteration of apoB-100 conformation. These structural changes of apoB-100 could largely result from the ability of the amphipathic peptides to strongly bind to and/or sequester lipids on the surface of LDL particles (17, 20), thus perturbing lipid distribution in LDL surfaces that consequently modulate apoB-100 conformation. Using lipid trilayers to mimic the protein-free LDL, our atomistic simulation data clearly indicated that 4F bound and inserted into LDL lipids and subsequently induced changes in lipid organization in the system. A deep free energy minimum is located at the trilayer surface in the case of both unmodified and SMase-treated LDL, and the adsorption of 4F to the membrane surface has a strong contribution due to electrostatics, presumably complemented by the hydrophobic effect. The electrostatic binding is the strongest prior to SMase treatment but remains strong also after the treatment. The binding of 4F to the lipids at the LDL surface reduces the conformational order of the lipids that are in the vicinity of 4F, but the peptide increases the lipids' order outside the 4F binding region, thereby rendering the membrane more compressed overall.


The perturbation of lipids in LDL particles upon interactions with 4F has been supported by our experimental data showing that LDL particles are less susceptible to SMase, an enzyme known to be sensitive to lipid perturbation (44). Thus, the conformational shift of apoB-100 following 4F interaction is consistent with the results of previous studies revealing conformational flexibility of apoB-100 (45) and also agrees well with the evidence demonstrating lipid-dependent structural changes in specific domains of apoB-100 (46). Additionally, although to a much smaller degree, we could not rule out the possibility that the local structural changes in apoB-100 structure might also be related to an ability of 4F to bind directly to domains of apoB-100 exposed on the LDL surface. Similarly, 17 β -estradiol has been shown to affect conformational properties of apoB-100 by binding to its specific domain, thereby stabilizing LDL particles and also preventing LDL aggregation in the presence of electronegative LDL (47, 48).

Interestingly, high concentrations of 4F caused dramatic changes in LDL particles, resulting in partial destabilization

of the particles, in an increase in LDL particle size (Fig. 6A, B), and in a decrease in the binding of LDL to LDL receptor (supplementary Fig. 6). Such a destabilizing effect on LDL could be largely related to membrane-lysing activity of amphipathic peptides as a result of its pore formation at high concentrations (49, 50). As the concentration of 4F increases, the peptide might undergo a dynamic reorientation relative to LDL lipid monolayer, resulting in the destruction of LDL lipid packing and, eventually, destabilization of LDL particles.

Therefore, we aimed at conditions in which concentrations required to protect SMase-induced LDL aggregation did not induce total changes in structure of LDL (i.e., molar ratio of 4F to apoB-100 below 20:1). Of note, 4F at concentrations used in the present study has been demonstrated to exhibit its antiatherosclerotic properties in mice (20, 51) and to improve functional properties of HDL in human plasma (10, 52, 53). Relevantly, 4F effectively blocked SMase-induced LDL aggregation regardless of whether 4F was added to partially aggregated LDL, whether 4F was present during incubation, or whether unbound 4F had been removed before SMase modification of LDL. Moreover, 4F blocked SMase-induced LDL aggregation both at neutral and acidic pH, suggesting that hydrophobic interactions between 4F and LDL particles were also of importance (54). SMase-induced aggregation of LDL has been shown to depend on the exposure and subsequent mutual interactions of hydrophobic domains of apoB-100 that are buried in native LDL particles (26). Thus, we envision that 4F, when present during treatment of LDL with SMase or after it, when aggregation of LDL particles has already partially taken place, blocks SMase-induced aggregation by interfering with the interactions between the exposed hydrophobic areas of SMase-modified LDL particles that are responsible for their aggregation. In analogy, amphipathic α -helix-containing proteins and HDL particles have been shown to block LDL aggregation, possibly by masking hydrophobic interactions between vortexed or PLC-modified LDL particles (21, 22). Indeed, when added to partly aggregated LDL, 4F impeded aggregated LDL from further aggregation but, on the other hand, failed to disassemble the LDL aggregates. Interestingly, 4F did not have any effect on completely aggregated LDL particles, consistent with previous finding showing that amphipathic α -helix-containing apoA-I also failed to revert PLC-induced LDL aggregation (22). Thus, an additional important factor underlying the protection of 4F against SMase-induced LDL aggregation can be also related to interactions between 4F and nonaggregated LDL particles. This interaction could stabilize the nonaggregated particles, thereby suppressing them from further SMase-induced modification. Indeed, our results deriving from experimental conditions in which unbound 4F was removed before SMase modification (Figs. 3, 6C, and 7) indicate the importance of stable conformational shift of apoB-100 upon interactions with 4F in determining the peptide's ability to suppress SMase-induced LDL aggregation. In addition, the binding of 4F to LDL particles also prevents SMase from hydrolyzing the SM in LDL particles

possibly by local steric hindrance and/or via long-range effects on lipid perturbation as evidenced by enzyme kinetics and simulation data. The exact nature of the interaction between 4F and LDL particles and the molecular characteristics of the interactive domains of apoB-100 remain to be defined in future studies. Finally, it is important to note that in previous studies (21, 22), amphipathic α -helix-containing proteins were either present during initial perturbation or present in partially aggregated LDL containing both nonaggregated and aggregated LDL particles; thus, their protective action could also have depended on their capacity to affect structural features of LDL particles.

With respect to molecular mechanisms of action of 4F, initial studies (14, 55) suggested that the biological effects of 4F involve remodeling of HDL particles in the plasma compartment. However, recent studies (56, 57) have indicated that the antiatherogenic properties of 4F are largely due to its ability to modulate the level of oxidized phospholipids in the intestine. Because the mechanisms by which 4F exerts antiatherogenic properties is extremely complex (57, 58), it is likely that 4F may function through multiple mechanisms and that combination of these properties may be responsible for the net in vivo atheroprotection. In the present study, we have demonstrated that 4F suppresses the binding of SMase-modified LDL to proteoglycans, thereby providing a novel mechanism for antiatherogenic properties of 4F. The physiological relevance of the present study has been supported by our ex vivo data demonstrating that LDL isolated from L-4F-treated mice was less susceptible to SMase-induced aggregation. SMase modification perturbs the well-organized surface structure of LDL and generates modified particles with enhanced affinity to proteoglycans (59). Indeed, SMase has been demonstrated to play a critical role in the retention of LDL particles and so contribute to the development of atherosclerotic lesions (3, 7, 8). In summary, the data indicate that following interactions with LDL particles, 4F alters lipid organization in LDL particles, which subsequently induces a stable conformational shift in apoB-100, thereby conferring LDL particles with the ability to resist SMase-induced LDL aggregation and so block the binding of SMase-modified LDLs to proteoglycans. 

Note added in proof

The authors of this manuscript informed the *Journal* there were errors in their original supplemental data file that was uploaded, specifically in the section titled "Relaxation of the LDL trilayers to experimental surface pressure prior to peptide insertion" (page 2 of the supplemental data file) and the list of references (page 8). Following Editors-in-Chief and Associate Editor approval of these changes, the supplemental data file for this manuscript has been replaced online and has therefore changed from the supplemental data file that was originally accepted as associated with this manuscript. For full details on the changes that have been made to the supplemental data file, please contact the corresponding author.

The authors thank Maija Atuegwu and Mari Jokinen for excellent technical assistance and Dr. Tero Pihlajamaa for his valuable comments and help in circular dichroism spectroscopy.

REFERENCES

- Skälén, K., M. Gustafsson, E. K. Rydberg, L. M. Hulthen, O. Wiklund, T. L. Innerarity, and J. Boren. 2002. Subendothelial retention of atherogenic lipoproteins in early atherosclerosis. *Nature*. **417**: 750–754.
- Tabas, I., K. J. Williams, and J. Boren. 2007. Subendothelial lipoprotein retention as the initiating process in atherosclerosis: update and therapeutic implications. *Circulation*. **116**: 1832–1844.
- Oörni, K., M. O. Pentikainen, M. Ala-Korpela, and P. T. Kovanen. 2000. Aggregation, fusion, and vesicle formation of modified low density lipoprotein particles: molecular mechanisms and effects on matrix interactions. *J. Lipid Res.* **41**: 1703–1714.
- Oörni, K., P. Posio, M. Ala-Korpela, M. Jauhiainen, and P. T. Kovanen. 2005. Sphingomyelinase induces aggregation and fusion of small very low-density lipoprotein and intermediate-density lipoprotein particles and increases their retention to human arterial proteoglycans. *Arterioscler. Thromb. Vasc. Biol.* **25**: 1678–1683.
- Marathe, S., S. L. Schissel, M. J. Yellin, N. Beatini, R. Mintzer, K. J. Williams, and I. Tabas. 1998. Human vascular endothelial cells are a rich and regulatable source of secretory sphingomyelinase. Implications for early atherogenesis and ceramide-mediated cell signaling. *J. Biol. Chem.* **273**: 4081–4088.
- Schissel, S. L., E. H. Schuchman, K. J. Williams, and I. Tabas. 1996. Zn²⁺-stimulated sphingomyelinase is secreted by many cell types and is a product of the acid sphingomyelinase gene. *J. Biol. Chem.* **271**: 18431–18436.
- Schissel, S. L., J. Tweedie-Hardman, J. H. Rapp, G. Graham, K. J. Williams, and I. Tabas. 1996. Rabbit aorta and human atherosclerotic lesions hydrolyze the sphingomyelin of retained low-density lipoprotein. Proposed role for arterial-wall sphingomyelinase in subendothelial retention and aggregation of atherogenic lipoproteins. *J. Clin. Invest.* **98**: 1455–1464.
- Devlin, C. M., A. R. Leventhal, G. Kuriakose, E. H. Schuchman, K. J. Williams, and I. Tabas. 2008. Acid sphingomyelinase promotes lipoprotein retention within early atheromata and accelerates lesion progression. *Arterioscler. Thromb. Vasc. Biol.* **28**: 1723–1730.
- Anantharamaiah, G. M. 1986. Synthetic peptide analogs of apolipoproteins. *Methods Enzymol.* **128**: 627–647.
- Navab, M., G. M. Anantharamaiah, S. T. Reddy, S. Hama, G. Hough, V. R. Grijalva, N. Yu, B. J. Ansell, G. Datta, D. W. Garber, et al. 2005. Apolipoprotein A-I mimetic peptides. *Arterioscler. Thromb. Vasc. Biol.* **25**: 1325–1331.
- Navab, M., G. M. Anantharamaiah, S. T. Reddy, and A. M. Fogelman. 2006. Apolipoprotein A-I mimetic peptides and their role in atherosclerosis prevention. *Nat. Clin. Pract. Cardiovasc. Med.* **3**: 540–547.
- Getz, G. S., and C. A. Reardon. 2011. Apolipoprotein A-I and A-I mimetic peptides: a role in atherosclerosis. *J. Inflamm. Res.* **4**: 83–92.
- Anantharamaiah, G. M., V. K. Mishra, D. W. Garber, G. Datta, S. P. Handattu, M. N. Palgunachari, M. Chaddha, M. Navab, S. T. Reddy, J. P. Segrest, et al. 2007. Structural requirements for antioxidative and anti-inflammatory properties of apolipoprotein A-I mimetic peptides. *J. Lipid Res.* **48**: 1915–1923.
- Navab, M., G. M. Anantharamaiah, S. T. Reddy, S. Hama, G. Hough, V. R. Grijalva, A. C. Wagner, J. S. Frank, G. Datta, D. Garber, et al. 2004. Oral D-4F causes formation of pre-beta high-density lipoprotein and improves high-density lipoprotein-mediated cholesterol efflux and reverse cholesterol transport from macrophages in apolipoprotein E-null mice. *Circulation*. **109**: 3215–3220.
- Li, X., K. Y. Chyu, J. R. Faria Neto, J. Yano, N. Nathwani, C. Ferreira, P. C. Dimayuga, B. Cercek, S. Kaul, and P. K. Shah. 2004. Differential effects of apolipoprotein A-I-mimetic peptide on evolving and established atherosclerosis in apolipoprotein E-null mice. *Circulation*. **110**: 1701–1705.
- Berliner, J. A., N. Leitinger, and S. Tsimikas. 2009. The role of oxidized phospholipids in atherosclerosis. *J. Lipid Res.* **50** (Suppl.): S207–S212.
- Van Lenten, B. J., A. C. Wagner, C. L. Jung, P. Ruchala, A. J. Waring, R. I. Lehrer, A. D. Watson, S. Hama, M. Navab, G. M. Anantharamaiah, et al. 2008. Anti-inflammatory apoA-I-mimetic peptides bind oxidized lipids with much higher affinity than human apoA-I. *J. Lipid Res.* **49**: 2302–2311.
- Navab, M., S. Y. Hama, C. J. Cooke, G. M. Anantharamaiah, M. Chaddha, L. Jin, G. Subbanagounder, K. F. Faull, S. T. Reddy, N. E. Miller, et al. 2000. Normal high density lipoprotein inhibits three steps in the formation of mildly oxidized low density lipoprotein: step 1. *J. Lipid Res.* **41**: 1481–1494.
- Navab, M., J. A. Berliner, G. Subbanagounder, S. Hama, A. J. Lusis, L. W. Castellani, S. Reddy, D. Shih, W. Shi, A. D. Watson, et al. 2001. HDL and the inflammatory response induced by LDL-derived oxidized phospholipids. *Arterioscler. Thromb. Vasc. Biol.* **21**: 481–488.
- Meriwether, D., S. Imaizumi, V. Grijalva, G. Hough, L. Vakili, G. M. Anantharamaiah, R. Farias-Eisner, M. Navab, A. M. Fogelman, S. T. Reddy, et al. 2011. Enhancement by LDL of transfer of L-4F and oxidized lipids to HDL in C57BL/6J mice and human plasma. *J. Lipid Res.* **52**: 1795–1809.
- Khoo, J. C., E. Miller, P. McLoughlin, and D. Steinberg. 1990. Prevention of low density lipoprotein aggregation by high density lipoprotein or apolipoprotein A-I. *J. Lipid Res.* **31**: 645–652.
- Liu, H., D. G. Scraba, and R. O. Ryan. 1993. Prevention of phospholipase-C induced aggregation of low density lipoprotein by amphipathic apolipoproteins. *FEBS Lett.* **316**: 27–33.
- Datta, G., M. Chaddha, S. Hama, M. Navab, A. M. Fogelman, D. W. Garber, V. K. Mishra, R. M. Epanand, R. F. Epanand, S. Lund-Katz, et al. 2001. Effects of increasing hydrophobicity on the physical-chemical and biological properties of a class A amphipathic helical peptide. *J. Lipid Res.* **42**: 1096–1104.
- Havel, R. J., H. A. Eder, and J. H. Bragdon. 1955. The distribution and chemical composition of ultracentrifugally separated lipoproteins in human serum. *J. Clin. Invest.* **34**: 1345–1353.
- Tong, H., H. R. Knapp, and M. VanRollins. 1998. A low temperature flotation method to rapidly isolate lipoproteins from plasma. *J. Lipid Res.* **39**: 1696–1704.
- Sneck, M., S. D. Nguyen, T. Pihlajamaa, G. Yohannes, M. L. Riekkola, R. Milne, P. T. Kovanen, and K. Oorni. 2012. Conformational changes of apoB-100 in SMase-modified LDL mediate formation of large aggregates at acidic pH. *J. Lipid Res.* **53**: 1832–1839.
- Nguyen, S. D., K. Oorni, M. Lee-Rueckert, T. Pihlajamaa, J. Metso, M. Jauhiainen, and P. T. Kovanen. 2012. Spontaneous remodeling of HDL particles at acidic pH enhances their capacity to induce cholesterol efflux from human macrophage foam cells. *J. Lipid Res.* **53**: 2115–2125.
- Hurt-Camejo, E., G. Camejo, B. Rosengren, F. Lopez, O. Wiklund, and G. Bondjers. 1990. Differential uptake of proteoglycan-selected subfractions of low density lipoprotein by human macrophages. *J. Lipid Res.* **31**: 1387–1398.
- Oörni, K., M. O. Pentikainen, A. Annala, and P. T. Kovanen. 1997. Oxidation of low density lipoprotein particles decreases their ability to bind to human aortic proteoglycans. Dependence on oxidative modification of the lysine residues. *J. Biol. Chem.* **272**: 21303–21311.
- Mishra, V. K., G. M. Anantharamaiah, J. P. Segrest, M. N. Palgunachari, M. Chaddha, S. W. Sham, and N. R. Krishna. 2006. Association of a model class A (apolipoprotein) amphipathic alpha helical peptide with lipid: high resolution NMR studies of peptide.lipid discoidal complexes. *J. Biol. Chem.* **281**: 6511–6519.
- Lehtonen, J. V., D. J. Still, V. V. Rantanen, J. Ekholm, D. Bjorklund, Z. Iftikhar, M. Huhtala, S. Repo, A. Jussila, J. Jaakkola, et al. 2004. BODIL: a molecular modeling environment for structure-function analysis and drug design. *J. Comput. Aided Mol. Des.* **18**: 401–419.
- Jämbeck, J. P., and A. P. Lyubartsev. 2012. Derivation and systematic validation of a refined all-atom force field for phosphatidylcholine lipids. *J. Phys. Chem. B.* **116**: 3164–3179.
- Jämbeck, J. P. M., and A. P. Lyubartsev. 2013. Another piece of the membrane puzzle: extending Slipids further. *J. Chem. Theory Comput.* **9**: 774–784.
- Jämbeck, J. P. M., and A. P. Lyubartsev. 2012. An extension and further validation of an all-atomistic force field for biological membranes. *J. Chem. Theory Comput.* **8**: 2938–2948.
- Jorgensen, W. L., J. Chandrasekhar, J. D. Madura, R. W. Impey, and M. L. Klein. 1983. Comparison of simple potential functions for simulating liquid water. *J. Chem. Phys.* **79**: 926–935.
- Pronk, S., S. Pall, R. Schulz, P. Larsson, P. Bjelkmar, R. Apostolov, M. R. Shirts, J. C. Smith, P. M. Kasson, D. van der Spoel, et al. 2013. GROMACS 4.5: a high-throughput and highly parallel open source molecular simulation toolkit. *Bioinformatics.* **29**: 845–854.

37. Hevonoja, T., M. O. Pentikainen, M. T. Hyvonen, P. T. Kovanen, and M. Ala-Korpela. 2000. Structure of low density lipoprotein (LDL) particles: basis for understanding molecular changes in modified LDL. *Biochim. Biophys. Acta.* **1488**: 189–210.
38. Gapsys, V., B. L. de Groot, and R. Briones. 2013. Computational analysis of local membrane properties. *J. Comput. Aided Mol. Des.* **27**: 845–858.
39. Hub, J. S., B. L. de Groot, and D. van der Spoel. 2010. g_wham—a free weighted histogram analysis implementation including robust error and autocorrelation estimates. *J. Chem. Theory Comput.* **6**: 3713–3720.
40. Datta, G., R. F. Epanand, R. M. Epanand, M. Chaddha, M. A. Kirksey, D. W. Garber, S. Lund-Katz, M. C. Phillips, S. Hama, M. Navab, et al. 2004. Aromatic residue position on the nonpolar face of class A amphipathic helical peptides determines biological activity. *J. Biol. Chem.* **279**: 26509–26517.
41. Best, R. B., N. V. Buchete, and G. Hummer. 2008. Are current molecular dynamics force fields too helical? *Biophys. J.* **95**: L07–L09.
42. Hornak, V., R. Abel, A. Okur, B. Strockbine, A. Roitberg, and C. Simmerling. 2006. Comparison of multiple Amber force fields and development of improved protein backbone parameters. *Proteins.* **65**: 712–725.
43. Gorbenko, G., T. Handa, H. Saito, J. Molotkovsky, M. Tanaka, M. Egashira, and M. Nakano. 2003. Effect of cholesterol on bilayer location of the class A peptide Ac-18A-NH₂ as revealed by fluorescence resonance energy transfer. *Eur. Biophys. J.* **32**: 703–709.
44. Goñi, F. M., and A. Alonso. 2002. Sphingomyelinases: enzymology and membrane activity. *FEBS Lett.* **531**: 38–46.
45. Wang, L., M. T. Walsh, and D. M. Small. 2006. Apolipoprotein B is conformationally flexible but anchored at a triolein/water interface: a possible model for lipoprotein surfaces. *Proc. Natl. Acad. Sci. USA.* **103**: 6871–6876.
46. Chauhan, V., X. Wang, T. Ramsamy, R. W. Milne, and D. L. Sparks. 1998. Evidence for lipid-dependent structural changes in specific domains of apolipoprotein B100. *Biochemistry.* **37**: 3735–3742.
47. Brunelli, R., G. Greco, M. Barteri, E. K. Krasnowska, G. Mei, F. Natella, A. Pala, S. Rotella, F. Ursini, L. Zichella, et al. 2003. One site on the apoB-100 specifically binds 17-beta-estradiol and regulates the overall structure of LDL. *FASEB J.* **17**: 2127–2129.
48. Brunelli, R., G. Balogh, G. Costa, M. De Spirito, G. Greco, G. Mei, E. Nicolai, L. Vigh, F. Ursini, and T. Parasassi. 2010. Estradiol binding prevents ApoB-100 misfolding in electronegative LDL. *Biochemistry.* **49**: 7297–7302.
49. Epanand, R. M., Y. Shai, J. P. Segrest, and G. M. Anantharamaiah. 1995. Mechanisms for the modulation of membrane bilayer properties by amphipathic helical peptides. *Biopolymers.* **37**: 319–338.
50. Sato, H., and J. B. Feix. 2006. Peptide-membrane interactions and mechanisms of membrane destruction by amphipathic alpha-helical antimicrobial peptides. *Biochim. Biophys. Acta.* **1758**: 1245–1256.
51. Navab, M., S. T. Reddy, G. M. Anantharamaiah, G. Hough, G. M. Buga, J. Danciger, and A. M. Fogelman. 2012. D-4F-mediated reduction in metabolites of arachidonic and linoleic acids in the small intestine is associated with decreased inflammation in low-density lipoprotein receptor-null mice. *J. Lipid Res.* **53**: 437–445.
52. Troutt, J. S., W. E. Alborn, M. K. Mosior, J. Dai, A. T. Murphy, T. P. Beyer, Y. Zhang, G. Cao, and R. J. Konrad. 2008. An apolipoprotein A-I mimetic dose-dependently increases the formation of prebeta HDL in human plasma. *J. Lipid Res.* **49**: 581–587.
53. Watson, C. E., N. Weissbach, L. Kjems, S. Ayalasomayajula, Y. Zhang, I. Chang, M. Navab, S. Hama, G. Hough, S. T. Reddy, et al. 2011. Treatment of patients with cardiovascular disease with L-4F, an apoA-I mimetic, did not improve select biomarkers of HDL function. *J. Lipid Res.* **52**: 361–373.
54. Sparrow, J. T., and A. M. Gotto, Jr. 1982. Apolipoprotein/lipid interactions: studies with synthetic polypeptides. *CRC Crit. Rev. Biochem.* **13**: 87–107.
55. Wool, G. D., C. A. Reardon, and G. S. Getz. 2008. Apolipoprotein A-I mimetic peptide helix number and helix linker influence potentially anti-atherogenic properties. *J. Lipid Res.* **49**: 1268–1283.
56. Navab, M., S. T. Reddy, G. M. Anantharamaiah, S. Imaizumi, G. Hough, S. Hama, and A. M. Fogelman. 2011. Intestine may be a major site of action for the apoA-I mimetic peptide 4F whether administered subcutaneously or orally. *J. Lipid Res.* **52**: 1200–1210.
57. Navab, M., S. T. Reddy, B. J. Van Lenten, G. M. Buga, G. Hough, A. C. Wagner, and A. M. Fogelman. 2012. High-density lipoprotein and 4F peptide reduce systemic inflammation by modulating intestinal oxidized lipid metabolism: novel hypotheses and review of literature. *Arterioscler. Thromb. Vasc. Biol.* **32**: 2553–2560.
58. White, C. R., D. W. Garber, and G. M. Anantharamaiah. 2014. Anti-inflammatory and cholesterol-reducing properties of apolipoprotein mimetics: a review. *J. Lipid Res.* **55**: 2007–2021.
59. Oörmi, K., J. K. Hakala, A. Annala, M. Ala-Korpela, and P. T. Kovanen. 1998. Sphingomyelinase induces aggregation and fusion, but phospholipase A2 only aggregation, of low density lipoprotein (LDL) particles. Two distinct mechanisms leading to increased binding strength of LDL to human aortic proteoglycans. *J. Biol. Chem.* **273**: 29127–29134.